JOURNAL OF GEOPHYSICAL RESEARCH, VOL. 102, NO. D16, PAGES 19,629–19,643, AUGUST 27, 1997

A dynamic water vapor correction method for the retrieval of land surface temperatures from the advanced very high resolution radiometer

Moira L. Steyn-Ross and D. Alistair Steyn-Ross

Department of Physics and Electronic Engineering, University of Waikato, Hamilton, New Zealand

W. J. Emery

Department of Aerospace Engineering Sciences, University of Colorado, Boulder

Abstract. We present a method which permits retrievals of land surface temperatures (LSTs) from AVHRR (advanced very high resolution radiometer) radiances sensed through atmospheres which may contain a large and strongly varying water vapor content. This new method is an extension of the dynamic water vapor (DWV) algorithm which was designed to retrieve sea surface temperatures. The generalization to LST retrievals recognizes that in general, land emissivities are unknown, may be spectrally dependent, and are less than unity. Because the LST retrieval problem is inherently underconstrained (there are more unknowns than radiative transfer equations), some knowledge of surface emissivity is required in order to establish upper and lower bounds on surface temperature. We demonstrate our method by comparing DWV-LST retrievals with point surface measurements made by a cluster of eight infrared thermometers (IRTs) deployed over a grasslands prairie site in eastern Kansas in July and August 1989; this deployment was part of the First International Satellite Land Surface Climatology Project (ISLSCP) Field Experiment (FIFE). We find that several of the AVHRR images supplied on FIFE CD-ROM contain navigation errors of ~30 km, consistent with a misidentification of the Tuttle Reservoir ground control point. After correcting the navigation, we identified the IRT pixels and computed the bias and rms errors for a DWV-IRT comparison. For night passes we obtained agreement to $+0.39 \pm 1.11$ K, while for day passes the comparison yielded $+4.09 \pm 3.10$ K. The large daytime bias is probably the result of the IRT readings not being representative of the ~1 km^2-scale areas sensed by AVHRR (the IRT views vegetation; the AVHRR field of view includes warmer, less well vegetated surfaces). Our results show that while a fixed-coefficient, global split-window algorithm does not perform well in the relatively moist FIFE atmosphere, it is quite feasible to use the DWV-LST to derive a local split-window algorithm whose coefficient is tuned on a per-pass basis.

1. Introduction

The thermal infrared channels of the advanced very high resolution radiometer, AVHRR, (channel 4: 10.8 μm; channel 5: 11.9 μm) have been used successfully to measure sea surface temperatures (SSTs) for well over a decade. Operational SST algorithms are based on the so-called "split-window" principle first derived by *Anding and Kauth* [1970], and subsequently developed by *Prabhakara et al.* [1974] and *McMillin* [1975]. This principle asserts that using a pair of radiance measurements taken at two wavelengths within the same atmospheric transmission window, one can compute a differential brightness temperature correction which largely eliminates atmospheric effects. Thus the simplest split-window algorithm takes the form

$$T_s = T_4 + a(T_4 - T_5) \tag{1}$$

where T_s is the surface temperature, T_4 and T_5 are the brightness temperatures in AVHRR channels 4 and 5 measured at the satellite, and the coefficient a is a regression-fitted constant.

The retrieval of land surface temperatures (LSTs) from satellite infrared radiometry is a more challenging problem than the corresponding surface temperature retrieval over sea. Ignoring the vexing question of just what defines the radiating surface (canopy, stem, soil?), there is the difficulty that unlike the sea surface,

Copyright 1997 by the American Geophysical Union

Paper number 97JD00776.
0148-0227/97/97JD-00776$09.00

the effective infrared emissivity of land surface is generally unknown, and can be smaller than unity. Thus the ground acts like a grey body radiator rather than an ideal blackbody. This means that in addition to its radiated energy, the infrared signal from the ground will contain a small component arising from the reflection of the downwelling sky radiance in the imperfect land mirror. The ground signal arriving at the radiometer will have been attenuated by the intervening atmosphere, and augmented by upwelling sky radiance emitted into the slant path from ground to satellite.

Many workers have examined the practicality of retrieving LSTs from AVHRR [*Prata*, 1993, 1994; *Price*, 1984; *Becker and Li*, 1990; *Sobrino and Caselles*, 1991; *Sobrino et al.*, 1991; *Cooper and Asrar*, 1989; *Vidal*, 1991; *Ottle and Vidal-Madjar*, 1992; *Li and Becker*, 1993]. *Prata* [1993] gave a comprehensive review of the various methods used by these authors. Recent work by *Harris and Mason* [1992] and *Sobrino et al.* [1993, 1994] has corrected for atmospheric fluctuations by formulating a split-window algorithm whose coefficients depend on the ratio of transmittances in channels 4 and 5.

In principle, given a pair of at-satellite radiances in channels 4 and 5, an LST algorithm must solve the equations of transfer for surface temperature. The two channels provide two equations, but there are five unknowns: surface temperature, surface emissivities ε_4 and ε_5, corresponding to the frequencies of channels 4 and 5, and the atmospheric contributions to the at-satellite radiances of channels 4 and 5. To solve this underconstrained problem, some assumptions and additional information are required in order to reduce the number of unknowns.

The atmospheric contribution can be estimated by initializing an atmospheric transmission model, such as LOWTRAN-7 [*Kneizys et al.*, 1988], with local radiosondes or historical climatologies, thus reducing the number of unknowns to three: (ε_4, ε_5, T_s). If it is known that the emissivity is spectrally independent so that $\varepsilon_4 = \varepsilon_5 = \varepsilon$, then the retrieval problem becomes closed, since we now have two equations in two unknowns, (ε, T_s). Alternatively, we achieve closure if one or the other emissivity is known, or if the emissivity difference ($\varepsilon_4 - \varepsilon_5$) is known. If there is no knowledge of emissivity, it is impossible to retrieve T_s. This point was made lucidly by *Becker and Li* [1990].

It is generally accepted that in the 10–12 μm region, almost all soils and vegetation have emissivities which lie in the range $0.95 \leq \varepsilon \leq 0.99$, with dry sandy soils having values toward the lower end of this range, and vegetation at the upper end [*Salisbury and D'Aria*, 1992]. For the First International Satellite Land Surface Climatology Project (ISLSCP) Field Experiment (FIFE) grasslands prairie site, *Palluconi et al.* [1990] reported $\varepsilon = 0.99 \pm 0.01$, with very small (0.005) variation with wavelength between 8 and 12 μm. In constrast, *Blad et al.* [1990] found emissivity variations between 0.96 and 0.99 at FIFE.

The general LST retrieval scheme which we describe in the next section makes no a priori assumptions about emissivity, other than the fact that both ε_4 and ε_5 should be close to, but less than, unity, and very similar to each other. To test our algorithm, we compare our retrievals from AVHRR against point measurements made in 1989 during the fifth intensive field campaign (IFC5) of FIFE with infrared thermometers (IRTs) located at eight AMS (automatic meteorological station) sites. These IRT measurements assume a surface emissivity of unity; consequently for the present validation purposes our general scheme collapses to the simplified ideal case in which $\varepsilon_4 = \varepsilon_5 = 1.0$. This means that we are retrieving the effective brightness temperature of the (assumed black) ground, rather than the true thermodynamic surface temperature. Despite this simplification, the FIFE validation exercise provides a good demonstration of our method.

In the next section we describe the general dynamic water vapor (DWV) method and present the equations and a graphical interpretation of the retrieval scheme. In section 3 we describe the surface measurements, AVHRR imagery, and atmospheric soundings relevant to the FIFE site, and in section 4 we test the method by comparing our retrievals with the IRT point measurements. We discuss the performance of the method in terms of the bias and rms (root-mean-square) differences with respect to the IRT readings, and investigate its stability with respect to choice of radiosonde. In section 5 we illustrate how the DWV method can be used to derive a split-window algorithm whose coefficients are dynamically tuned on a per-satellite-pass basis.

2. The Dynamic Water Vapor Method

2.1. Philosophy

The scheme we are about to describe is a generalization of the dynamic water vapor method of *Steyn-Ross et al.* [1993], hereafter SR93. The SR93 method is a regression-free approach to the problem of retrieving accurate sea surface temperatures (SSTs) in the presence of strongly varying water vapor. The basic premise of SR93 is that if the atmospheric state (temperature and water vapor profile) is known, then, using LOWTRAN and the equations of transfer, the two at-satellite radiance measurements I_4, I_5 in AVHRR channels 4 and 5 can be inverted to produce a pair of independent SST predictions, SST_4 and SST_5. In the ideal case, the two predictions match, $SST_4 = SST_5$, and the actual surface temperature has been retrieved. More typically, $SST_4 \neq SST_5$, indicating that the first-guess atmosphere is in error. Since the most likely source of error is in the water vapor profile, we iterate the water column amount (either increasing or decreasing the water vapor loading) until the two SST estimates converge. When tested over coastal waters off the west coast of Tasmania, Australia, the SR93 algorithm returned SST estimates with an rms error of 0.6 K, and a bias of

±0.22 K (satellite SST underestimated buoy-measured bulk temperature by 0.22 K), which is within the skin effect uncertainty.

While it is intuitively obvious that over ocean targets the first-guess water vapor profile might need to be tuned before it is locally accurate, the need for water vapor tuning over land targets is less clear. In fact, there is evidence to suggest that water vapor profiles are strongly varying functions of terrain, vegetation, and time of day. *Bruegge et al.* [1992] made aircraft observations over the FIFE site with an AVIRIS (airborne visible infrared imaging spectrometer) instrument. From these observations they estimated that surface topography and vegetation produced variations in water column across the 15- by 15-km FIFE site of the order of 10%. This suggests that even if one has a temporally and spatially local radiosonde, fine-tuning of the water profile may still be required, since surface and upper level winds will cause the sounding balloon to drift sideways as it ascends.

The generalization of DWV to land targets proceeds as follows. We initialize an atmospheric transmission model (LOWTRAN-7) using a nearby radiosonde and use it to compute the atmospheric transmissivity, downwelling radiance, and upwelling radiance for AVHRR channels 4 and 5. From the two infrared radiance measurements in channels 4 and 5, we generate two equations of transfer in three unknowns: T_s, ε_4, ε_5. We invert these equations to give a pair of expressions for ε_4 and ε_5 as a function of surface temperature, and then plot the emissivity curves for a range of possible surface temperatures; see Figure 1. If the emissivity is independent of wavelength, then the two emissivity curves should intersect somewhere in the interval $0.95 \leq \varepsilon \leq 1.00$. If the intersection point lies outside this interval, the atmospheric sounding is assumed to be in error, and the water vapor profile is adjusted iteratively to bring the $\varepsilon_4/\varepsilon_5$ intersection point within range.

Figure 1 shows the range of possible solutions for the emissivities as a function of surface temperature for a particular sample atmosphere and pair of satellite radiances. Those parts of either curve which show an apparent emissivity greater than unity are immediately rejected as unphysical. Our region of interest lies in the vicinity of the intersection point, since field experiments have shown that land surface emissivities in channels 4 and 5 have values which do not differ by more than about 0.02, with both emissivities being less than, but not very different from, unity.

When the curves intersect at a point for which $\varepsilon_4 \leq 1.00$ and $\varepsilon_5 \leq 1.00$, we can have confidence in our assumed atmosphere and continue. Referring to the figure, note the temperature at which each curve passes through $\varepsilon = 1$. The larger of these two temperatures corresponds to the precise lower bound for T_s. (In the figure, this is the temperature at which $\varepsilon_5 = 1$.) Locating the upper bound for T_s requires some a priori

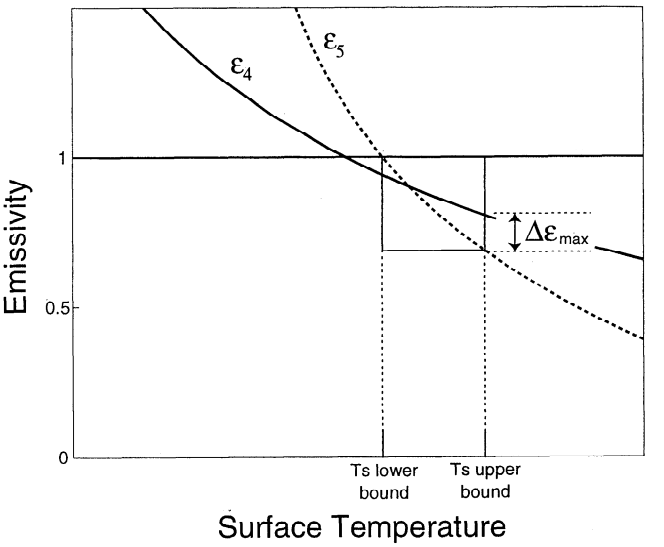

Figure 1. Schematic showing the emissivity trend (see equation (6)) as a function of surface temperature. Some knowledge of surface emissivity (or emissivity difference) is required to establish upper and lower bounds on the surface temperature.

knowledge about the land type and its characteristic emissivity difference, $\Delta\varepsilon = \varepsilon_4 - \varepsilon_5$. Prescribing a maximum value for $\Delta\varepsilon$ sets the upper limit for T_s. The rectangle in the figure shows the resulting upper and lower bounds for the surface emissivities and temperature. We should acknowledge that *Becker and Li* [1990] seem to have anticipated this graphical $\varepsilon_4/\varepsilon_5$ approach with their Figures 9, 12, and 13. The essential distinction between their work and ours is our willingness to adjust the water profile if the intersection region is unphysical.

2.2. Radiative Transfer Theory

We now give a brief derivation of the equations of transfer as applied to the DWV method. We assume clear cloudless skies, no scattering, azimuthal independence, and a land surface whose emissivity does not vary with view zenith angle. Under these conditions, the monochromatic radiation $I_\nu(\theta)$ at wavenumber ν reaching the radiometer along a slant path of zenith angle θ can be written as the sum of three terms representing the surface radiation, the reflection of the sky radiance in the surface, and the upward sky radiance [e.g., *Becker and Li*, 1990; *Prata*, 1993]:

$$I_\nu(\theta) = \left[\varepsilon_\nu B_\nu(T_s) + (1-\varepsilon_\nu)L_\nu^\downarrow\right]\tau_\nu(\theta) + I_\nu^\uparrow(\theta) \quad (2)$$

where $B_\nu(T_s)$ is the Planck function evaluated at wavenumber ν, surface temperature T_s; $\tau_\nu(\theta)$ is the transmittance along the slant path from surface to satellite; and $I_\nu^\uparrow(\theta)$ is the upwelling atmospheric radiance. The quantity $L_\nu^\downarrow$ is the downwelling sky radiance averaged over the upper hemisphere Ω:

$$L_\nu^\downarrow = \frac{1}{\pi}\int_\Omega I_\nu^\downarrow(\theta,\phi)\cos\theta\, d\Omega \quad (3)$$

with differential solid angle $d\Omega = \sin\theta\, d\theta\, d\phi$. Since we assume the sky radiance is independent of azimuthal angle ϕ, the expression for $L_\nu^\downarrow$ reduces to

$$L_\nu^\downarrow = 2\int_0^1 I_\nu^\downarrow\, \mu\, d\mu \approx 2\sum_{j=1}^{N} a_j \mu_j I_\nu^\downarrow(\mu_j) \qquad (4)$$

where $\mu = \cos\theta$, and the integration has been replaced by an $N = 5$-point Gaussian quadrature with weights a_j [*Press et al.*, 1992]. Previous authors [e.g., *Prata*, 1993] have assumed that the downwelling sky radiance is isotropic, so that the nadir path sky radiance $I_\nu^\downarrow(0)$ can be used in place of $L_\nu^\downarrow$. For dry atmospheres this is a reasonable approximation; however, for moist atmospheres we find that $I_\nu^\downarrow(0)$ underestimates $L_\nu^\downarrow$ by about 30%.

The total radiance measured by the radiometer in AVHRR channel i ($i = 4, 5$) is obtained by integrating (2) over the channel response function $f_i(\nu)$:

$$\begin{aligned} I_\nu(\theta) &= \int_0^\infty f_i(\nu)\, I_\nu(\theta)\, d\nu \\ &= \int_0^\infty f_i(\nu)\left[\left(\varepsilon_\nu B_\nu(T_s) + (1-\varepsilon_\nu)L_\nu^\downarrow\right)\cdot\right. \\ &\qquad \left.\tau_\nu(\theta) + I_\nu^\uparrow(\theta)\right]\, d\nu \end{aligned} \qquad (5)$$

Assuming that the surface emissivity is constant over the channel i bandwidth, we can replace ε_ν by ε_i and solve (5) to give a pair of equations for emissivity as a function of surface temperature:

$$\varepsilon_4 = \frac{I_4 - I_4^\uparrow - \tau_4 L_4^\downarrow}{\tau_4 B_4(T_s) - \tau_4 L_4^\downarrow} \qquad (6a)$$

$$\varepsilon_5 = \frac{I_5 - I_5^\uparrow - \tau_5 L_5^\downarrow}{\tau_5 B_5(T_s) - \tau_5 L_5^\downarrow} \qquad (6b)$$

where the individual terms in each numerator and denominator are to be interpreted as

$$\begin{aligned} I_4^\uparrow &= \int_0^\infty f_4(\nu)\, I_\nu^\uparrow(\theta)\, d\nu \\ &\approx \Delta\nu \sum_{k=1}^{N_4} f_{4,k}\, I_k^\uparrow(\theta) \end{aligned} \qquad (7a)$$

$$\begin{aligned} \tau_4 L_4^\downarrow &= \int_0^\infty f_4(\nu)\, \tau_\nu(\theta)\, L_\nu^\downarrow\, d\nu \\ &\approx \Delta\nu \sum_{k=1}^{N_4} f_{4,k}\, \tau_k(\theta)\, L_k^\downarrow \end{aligned} \qquad (7b)$$

$$\begin{aligned} \tau_4 B_4(T_s) &= \int_0^\infty f_4(\nu)\, \tau_\nu(\theta)\, B_\nu(T_s)\, d\nu \\ &\approx \Delta\nu \sum_{k=1}^{N_4} f_{4,k}\, \tau_k(\theta)\, B_k(T_s) \end{aligned} \qquad (7c)$$

with corresponding expressions for channel 5. The integrations have been replaced by summations whose frequency resolution is set to match the finest step size for LOWTRAN-7: $\Delta\nu = 5$ cm^{-1}. (We note that since the internal resolution of LOWTRAN is $\Delta\nu = 20$ cm^{-1}, we are using radiances and transmittances which have been interpolated by LOWTRAN to the finer resolution.) The discretized AVHRR channel response functions $f_{i,k}$ are obtained by resampling at 5-cm^{-1} intervals (then area renormalizing) the response functions for channels 4 and 5 published by the National Environmental Satellite Data and Information Service (NESDIS). For NOAA 11 AVHRR, the channel 4 and 5 spectral widths are 850–1020 cm^{-1} (9.8–11.8 μm) and 780–915 cm^{-1} (10.9–12.9 μm), giving filter functions containing $N_4 = 35$, $N_5 = 28$ entries, respectively. With little loss of accuracy, and a substantial reduction in LOWTRAN execution time, one can replace each filter function with an appropriately weighted pair of LOWTRAN wavenumbers which bracket the central wavenumber for the given channel. As pointed out by an anonymous reviewer, calculation of the downward radiance (equation (4)) requires five runs of LOWTRAN, but for high surface emissivities, this term contributes little and could be computed in a single run by using a diffusivity factor.

2.3. DWV Algorithm

We can now detail the steps for the DWV-LST algorithm.

1. Based on some prior knowledge of the surface classification, specify the emissivity condition which is to be used to identify T_s. For example, $\varepsilon_4 = \varepsilon_5 = 1$ would be appropriate both over water, and also over land if we were seeking the effective blackbody brightness temperature (which is the case for our FIFE validation); $\varepsilon_4 = \varepsilon_5 = 0.99$ might be a reasonable choice over vegetation; and $\varepsilon_4 = 0.96$, $\varepsilon_5 = 0.97$ might be reasonable over a particular type of bare soil. For definiteness in the following discussion, we will assume that we are requesting a common emissivity value $\varepsilon_4 = \varepsilon_5 = \varepsilon_{\text{req}}$.

2. For the given AVHRR pixel, determine the scan angle, and compute the at-satellite radiances I_4, I_5 using the in-flight count-to-radiance calibrations.

3. Select the first-guess atmospheric profile (altitude, pressure, temperature, water vapor).

4. Use LOWTRAN-7 to compute the six atmospheric terms in equations (7): $I_4^\uparrow$, $L_4^\downarrow$, τ_4, $I_5^\uparrow$, $L_5^\downarrow$, τ_5. This entails six LOWTRAN runs per AVHRR channel: one run for each of the five Gaussian angles to compute the downwelling radiance, plus a final run at the given scan angle for the upwelling radiance and upward transmittance.

5. Using equations (7), plot ε_4 and ε_5 for a range of possible surface temperatures, and locate the temperature and emissivity coordinate (T_x, ε_x) at which the two curves intersect. If $\varepsilon_x = \varepsilon_{\text{req}}$, then the surface temperature has been retrieved: $T_s = T_x$. If $\varepsilon_x \neq \varepsilon_{\text{req}}$, the first-guess atmosphere is in error, so adjust the water vapor profile by a small amount. For FIFE, it was

found that $\varepsilon_x > \varepsilon_{\text{req}}$ was an indicator that the water vapor loading needed to be increased, and conversely for $\varepsilon_x < \varepsilon_{\text{req}}$. The water vapor adjustment is done by adding (or subtracting) a small constant to the relative humidity at every pressure level, subject to the constraint that the humidity can never be larger than 100% (or smaller than 0%).

6. Iterate steps 4 and 5 until $\varepsilon_x = \varepsilon_{\text{req}}$.

There are two points that need to be made here. First, in step 5 we are searching for the root of the nonlinear equation in T_s:

$$\varepsilon_4(T_s) = \varepsilon_5(T_s) = \varepsilon_{\text{req}} \tag{8}$$

From equations (6) we see that $\varepsilon_4(T_s)$ and $\varepsilon_5(T_s)$ are highly nonlinear functions of T_s (in fact, hyperbolic functions of $B(T_s)$), so (8) is likely to have multiple roots, only one of which has physical meaning in the context of LST retrieval. Thus the algorithm must take all care to ensure it is not distracted by one or other of these spurious roots. Second, we found with the FIFE work that for the dry atmosphere afternoon passes (August 8, 9, 11), there was frequently no $\varepsilon_4/\varepsilon_5$ intersection at all. In these cases the curves came close to osculating (touching), with a typical closest approach difference of 0.003, but did not cross. By generalizing our root-searching routine to accept a near-osculation as a proxy for curve intersection, we were able to obtain sensible LST retrievals even for these pathological cases. From our emissivity sensitivity studies (see section 4.2.1) we estimate that an emissivity mismatch of 0.003 contributes less than 0.2 K to the uncertainty in retrieved surface temperature.

Figures 2a–2d illustrate how, for a typical FIFE retrieval, the (T_x, ε_x) intersection point evolves as the water vapor loading is steadily increased. Plotted as a function of relative humidity adjustment (Figures 3a and 3b), we see that the ε_x and T_x curves evolve in opposite senses: an increased humidity corresponds to a larger T_x and smaller ε_x.

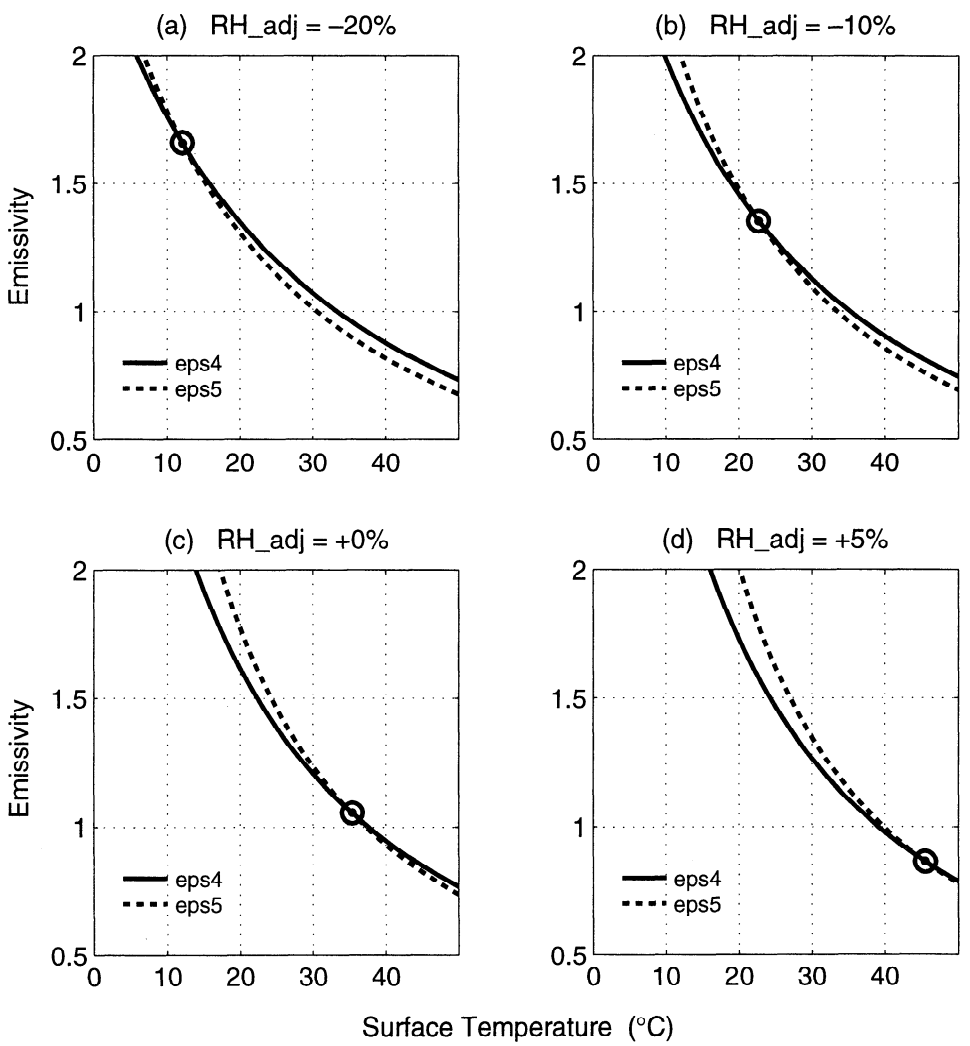

Figure 2. Emissivity versus surface temperature curves for a range of water vapor profile adjustments. These graphs illustrate step 5 of the DWV-LST algorithm (see text) applied to a single AVHRR FIFE pixel. As the water vapor loading is increased in Figures 2a through 2d, the $\varepsilon_4 = \varepsilon_5$ intersection point moves to lower emissivities and higher surface temperatures. RH_adj is the profile adjustment of relative humidity away from the first-guess (radiosonde) values.

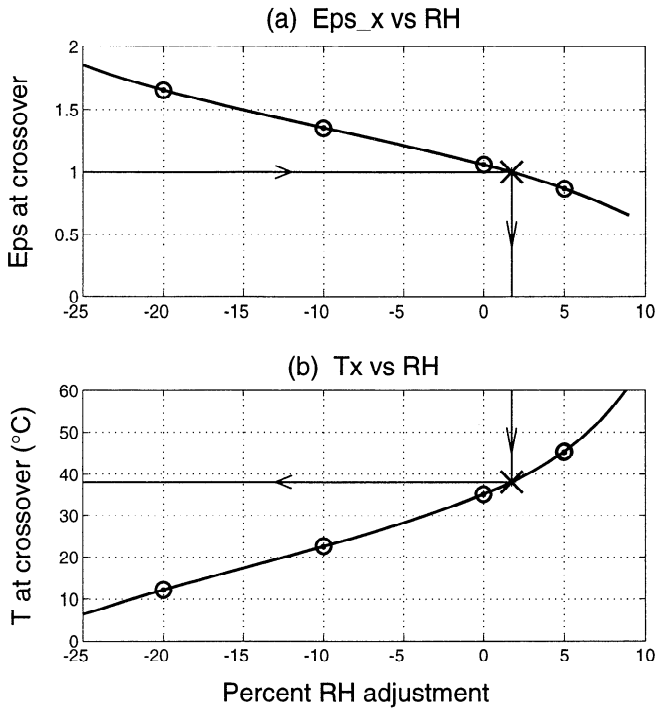

Figure 3. (a) Variation of equal-emissivity point ε_x with humidity adjustment. (b) Variation of equal-emissivity surface temperature T_x with humidity adjustment. Circled data come from the four intersection points shown in Figure 2. The arrows demonstrate a DWV-LST retrieval of $T_s = 38.1°C$ for an assumed common emissivity of $\varepsilon_x = 1.0$. (RH adjustment is defined in the Figure 2 caption.)

3. FIFE Data Sets

Field and satellite data used in the validation were gathered in July and August 1989 as part of the First International Satellite Land Surface Climatology Project (ISLSCP) Field Experiment (FIFE), and published as a set of five CD-ROMs [*Strebel et al.*, 1992, 1994]. The FIFE study area was a 15- by 15-km region of tallgrass prairie in eastern Kansas.

3.1. Infrared Thermometer Ground Sites

Eight automatic meteorological stations (AMSs) were located within the FIFE area, dispersed as shown in Figure 4, southeast quadrant. Each station recorded the apparent surface temperature using a nadir-looking infrared thermometer (IRT), of bandwidth 8–14 μm and measurement accuracy 0.3 K, calibrated for a surface emissivity of unity [*Stewart*, 1994]. The IRTs view an area of the ground of approximate diameter 0.5 m. Measurements were taken every 5 min and averaged over 30-min time intervals; we retrieved these 30-min averages from volume 1 of the FIFE CD-ROM set, and estimated the instantaneous temperature applicable to the satellite overpass by linearly interpolating between that pair of IRT measurements whose times bracketed the satellite overpass time. The interpolated IRT temperatures are shown in Table 1. Also shown in Table 1 are the AVHRR brightness temperatures in channels 4 and 5 for each image pixel which contains an IRT site.

It is interesting to note that for the night passes (0830 UT = 0330 local time) there is a 3°C-4°C range in surface temperatures across the land sites, while for the afternoon passes (2000 UT = 1500 LT) the ground temperatures are extremely heterogeneous, differing from one another by as much 16.5°C. When we consider that the area of the smallest AVHRR pixel (nadir, 1.1 km^2) is 5 million times larger than the spot sampled by an IRT, it becomes clear that the IRT point readings can, at best, provide only a weak proxy for the square kilometer-scale temperatures sensed by AVHRR.

For this reason, it is tempting to contemplate Tuttle Reservoir as a source of AVHRR-scale ground truth temperatures. The column labeled "Tuttle" in Table 1 shows the IRT-measured surface temperatures for Tuttle Reservoir. The coincidence criteria for inclusion in this table are that the Tuttle measurement must lie within 5 hours of the closest satellite night pass, or within 2 hours of the closest day pass. Compared with the nearby land sites, the water measurements are remarkably stable. Unfortunately, the very features

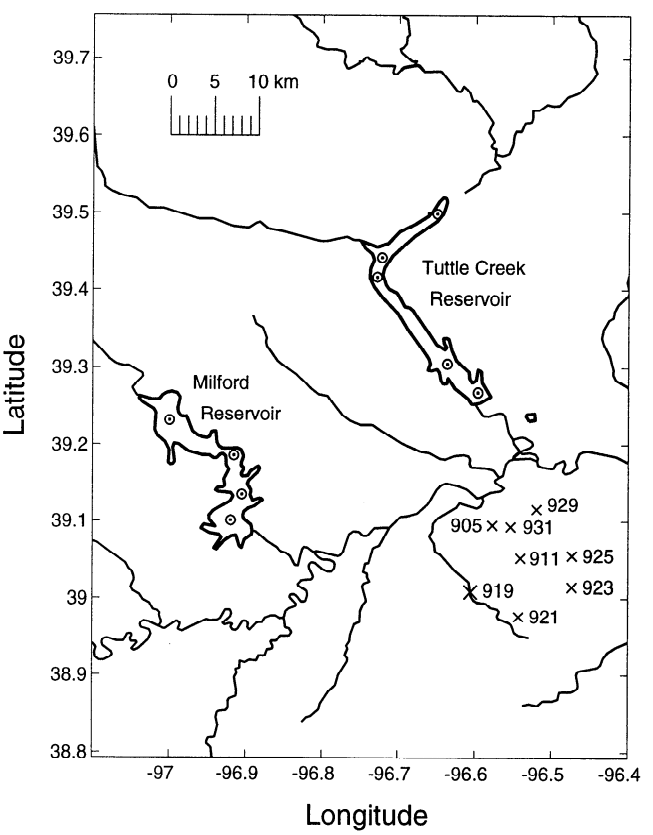

Figure 4. Map of the FIFE study area. Each of the eight IRT (infrared thermometer) sites is identified with a three-digit code 9nn. The circled points in the Tuttle Creek and Milford reservoirs define the suite of ground control points (GCPs) we used to renavigate the AVHRR images. (This map was prepared from data extracted from the Digital Chart of the World in ASCII [Ph.D. Associates, Inc., 1994].)

Table 1. Surface Temperatures and AVHRR Brightness Temperatures at FIFE-89 IRT Ground Sites and Tuttle Reservoir

Date in 1989	UT[a]	Variable	IRT Ground Site								Tuttle[b]		Mean[c]	sdev[c]
			905	911	919	921	923	925	929	931	First Datum	Second Datum		
Night Passes (Descending)														
July 28	0834	T_s	22.8	21.3	20.5	21.1	19.2	20.1	20.7	22.7	...	...	21.1	1.2
		T_4	18.6	18.4	18.6	18.6	18.2	18.8	19.0	18.6	20.7	20.9	18.6	0.2
		T_5	17.2	17.1	17.5	17.5	16.8	17.5	17.7	17.3	18.8	18.8	17.3	0.3
July 29	0824	T_s	23.6	22.4	22.1	22.2	20.7	21.2	21.7	23.2	...	...	22.1	1.0
		T_4	19.6	19.5	...	19.6	19.2	19.5	18.3	19.4	17.8	16.3	19.3	0.5
		T_5	18.3	18.3	...	18.3	18.0	18.1	16.4	18.0	15.8	13.9	17.9	0.7
Aug. 6	0841	T_s	17.6	18.6	16.6	17.7	16.5	15.9	18.1	20.2	26.2	...	17.6	1.4
		T_4	16.4	17.2	17.0	17.0	17.1	17.1	17.3	16.8	21.5	22.7	17.0	0.3
		T_5	16.0	16.9	16.8	16.8	16.8	16.8	17.1	16.7	20.2	21.3	16.7	0.3
Aug. 7	0831	T_s	13.0	13.4	12.1	12.6	11.5	11.8	12.9	10.7	...	...	12.2	0.9
		T_4	11.3	11.4	11.4	11.1	11.6	11.5	11.8	11.1	19.5	19.8	11.4	0.2
		T_5	10.9	11.1	11.1	10.7	11.3	11.2	11.6	10.9	17.6	18.1	11.1	0.3
Aug. 8	0821	T_s	10.9	11.7	9.3	10.3	10.1	9.7	12.8	8.8	25.3	...	10.4	1.3
		T_4	9.1	9.4	9.9	8.9	9.4	9.9	10.9	9.4	20.1	20.2	9.6	0.6
		T_5	9.1	9.2	9.7	8.8	9.3	9.7	10.7	9.4	18.9	19.0	9.5	0.6
Afternoon Passes (Ascending)														
July 28	2000	T_s	33.6	32.1	44.9	41.8	31.0	38.4	43.7	35.0	...	...	37.5	5.4
		T_4	24.5	30.3	32.7	30.8	30.2	31.1	33.9	30.4	24.9	23.6	30.5	2.8
		T_5	20.3	26.1	27.9	25.8	26.1	26.9	28.9	26.1	20.6	20.0	26.0	2.5
Aug. 4	2029	T_s	44.6	32.0	40.3	37.3	31.3	36.2	39.8	38.9	26.7	...	37.5	4.4
		T_4	34.1	30.5	32.5	31.9	29.4	30.3	32.4	31.5	31.9	29.3	31.6	1.5
		T_5	30.5	27.7	29.0	28.7	26.8	27.6	28.9	28.4	29.3	27.2	28.5	1.1
Aug. 6	2007	T_s	34.8	26.3	33.2	30.9	25.8	33.9	32.2	28.5	...	...	30.7	3.4
		T_4	28.3	25.8	29.3	27.3	23.4	25.0	26.8	25.9	22.1	21.7	26.5	1.9
		T_5	24.5	22.6	25.4	23.9	20.4	21.8	23.3	22.7	19.5	19.0	23.1	1.6
Aug. 7	1957	T_s	36.0	24.7	33.3	30.0	23.9	34.2	32.7	27.9	25.7	...	30.3	4.5
		T_4	33.6	30.5	34.2	32.1	28.7	29.3	32.7	30.8	24.6	24.2	31.5	2.0
		T_5	31.8	28.8	32.6	30.5	27.2	27.8	30.6	29.2	22.5	22.6	29.8	1.9
Aug. 8	1946	T_s	41.2	26.8	35.1	32.1	26.4	31.1	35.7	33.9	26.6	...	32.8	4.9
		T_4	35.5	29.6	36.2	28.9	27.4	...	30.4	31.5	26.7	24.4	31.4	3.3
		T_5	33.3	27.6	34.1	24.7	25.3	...	27.2	29.9	25.3	22.8	28.9	3.7
Aug. 9	1936	T_s	43.5	30.7	39.6	36.1	26.9	39.5	38.8	36.0	...	...	36.4	5.3
		T_4	35.6	33.0	36.7	35.0	30.7	33.4	36.3	33.4	26.4	23.2	34.3	2.0
		T_5	33.6	31.4	34.9	32.8	28.7	31.7	34.3	32.0	22.9	21.6	32.4	2.0
Aug. 11	1916	T_s	38.7	31.8	38.4	35.2	26.7	37.5	38.0	36.7	...	...	35.4	4.2
		T_4	...	...	...	...	...	...	...	...	...	...	...	...
		T_5	...	...	...	...	...	...	...	...	...	...	...	...

Data are given as degrees Celsius. Here, s.d. denotes standard deviation.

[a]Local time = UT − 0500.

[b]The T_4 and T_5 Tuttle temperatures are for the pair of GCP pixels shown in Figure 4 toward the southern end of Tuttle Reservoir. The T_s surface temperatures are IRT values recorded during a boat traverse of the reservoir.

[c]Tuttle readings are excluded from these statistics.

which make Tuttle Reservoir ideal for checking navigation (discussed below) of AVHRR imagery (its shape is long, narrow, and kinked) mitigate against its use as ground truth. In most of the AVHRR images, the reservoir is only one or two pixels wide, so it is not possible to retrieve confidently a water pixel which is uncontaminated by radiance from the landmasses which border the reservoir. This is particularly apparent in Table 1 for the afternoon pass of August 4 at 2029 UT. The satellite scan angle of 45° (see Table 2) foreshortens the

Table 2. Navigation Corrections for the IFC5 NOAA 11 Images

Date in 1989	UT[a]	Image Identifier	Scan Angle,[b] degrees	Δx, pixels	Δy, pixels	Comment
			Night Passes (Descending)			
July 28	0834	92090834	14.0	1	0	
July 29	0824	92100824	26.8	2	−4	Cirrus over IRT site 919
Aug. 6	0841	92180841	4.2	−18	−19	
Aug. 7	0831	92190831	18.4	−15	−19	
Aug. 8	0821	92200821	30.3	−11	−19	
			Afternoon Passes (Ascending)			
July 28	2000	92092000	19.7	−8	−22	
Aug. 4	2029	92162029	44.6	−1	−1	45° scan angle; 2 scan lines blank
Aug. 6	2007	92182007	27.7	−8	0	
Aug. 7	1957	92191957	15.2	−1	1	
Aug. 8	1946	92201946	0.7	2	0	Popcorn cloud over IRT site 925
Aug. 9	1936	92211936	13.7	0	0	
Aug. 11	1916	92231916	36.1	?	?	Too cloudy to navigate

[a]Local time = UT − 0500
[b]Angle at satellite of ground target with respect to nadir, averaged across all eight IRT sites listed in Table 1.

Tuttle Reservoir into a narrow ribbon, causing the the resulting at-satellite signal to be a mixture of radiances from (warm) land and (relatively cool) water.

3.2. AVHRR Imagery: Navigation and Calibration

For the fifth intensive field campaign (IFC5) of FIFE in July and August 1989, there are a total of 12 navigated 256-line by 256-pixel AVHRR NOAA 11 subimages, centered on the dam at the south end of Tuttle Reservoir, stored on volume 2 of the FIFE CD-ROM set. The navigation information is presented as a pair of latitude and longitude files, with one (latitude, longitude) coordinate per image pixel.

Because we wished to identify the eight individual pixels in each image which contain the eight IRT ground sites, we sought reassurance that the navigation was accurate. From the public domain Central Intelligence Agency (CIA) World Database II we extracted all geographical features whose coordinates lie within 400 km of the FIFE site, then identified which pixel the CIA feature belonged to by searching the subimage to find that pixel which minimized the great circle arc length from pixel coordinate to feature coordinate. In this way we built up a map (in raw line/pixel space) of the river features for the FIFE region, one map per image. We then superimposed the map on the AVHRR image to check that the albedo (channels 1, 2) and radiance (channels 3, 4, 5) features in the raw image agreed with the river features from the CIA database. The results were disconcerting: Four of the images showed navigation errors of about 30 km, three had errors of up to 8 km, and only four had navigation accuracies which lay within the expected tolerance of ±1 km. (The final, twelfth image was so cloudy that no ground features were discernible.)

We were not confident that the CIA database was completely up to date (it was created from maps drawn prior to 1972, and contained no information about reservoirs and dams), so we repeated the navigation quality check using the commercial "Digital Chart of the World (DCW) in ASCII" CD-ROM [*Ph.D. Associates, Inc.*, 1994], which is a single-volume, nonhierarchical, text version of the DCW relational database published on four CD-ROMs by the United States Defense Mapping Agency in 1992. From the DCW we extracted the inland shorelines for Tuttle Creek and Milford reservoirs, and defined nine ground control points (GCPs), five for Tuttle, four for Milford, shown in Figure 4. We constructed a set of DCW overlay maps. These new comparisons confirmed our earlier CIA database findings, and suggested a possible reason for the poor FIFE navigations: The original FIFE image processing was done using a single GCP, normally the Tuttle Creek Dam at the southern end of the reservoir. The four worst case navigation errors were consistent with a FIFE operator inadvertantly selecting the north end of the reservoir as the dam GCP.

Listed in Table 2 are our estimates for the required navigation corrections for each image, presented as Δx (positive to the right) and Δy (positive downward) pixel/line translations of a normally viewed image (north to top, east to right) relative to its FIFE-published (latitude, longitude) grid. We estimate that these corrections are accurate to ±1.5 pixels in x and y.

The calibration of the thermal channels (conversion from raw channel 4, 5 count to radiance) follows the

method described by *Steyn-Ross et al.* [1992], updated with recently obtained 1988 NOAA 11 prelaunch information.

3.3. Radiosondes

Standard meteorological radiosondes were launched daily at 1200 UT (0700 LT) from Dodge City, 340 km to the southwest of FIFE, and at 0000 UT (1900 LT the previous day) from Topeka, 70 km to the east of FIFE. A typical sounding contained 26 atmospheric readings (pressure, altitude, temperature, relative humidity) at the mandatory pressure levels between surface pressure and altitude ~26 km; we used the upper levels of the LOWTRAN-7 midlatitude summer standard atmosphere to top up each sounding to altitude 100 km to give an extended profile containing a maximum of 34 atmospheric readings.

For our initial runs, we used the topped-up Dodge City sondes as the first-guess atmosphere. Relative to the NOAA 11 overpass times on a given day, the Dodge City sonde was launched $3\,^1/_2$ hours after the the 0330 LT descending (night) satellite pass, and 8 hours prior to the 1500 LT ascending (afternoon) pass. For the radiosonde sensitivity tests, we replaced the Dodge City sondes with the Topeka sondes whose UT date matched that of the NOAA 11 image. This means that the night pass is matched with a sonde which is $8\,^1/_2$ hours old, and the afternoon pass with the same sonde which is now 20 hours old. A time series showing the total water column computed from the Dodge City and Topeka radiosondes is displayed in Figure 5.

These soundings were retrieved from volume 1 of the FIFE CD-ROM set. Also contained on this volume are local radiosondes launched at $1\,^1/_2$-hour intervals during daylight hours at the FIFE site [*Sugita and Brutsaert,* 1990]. These sondes sampled only the bottom 4–5 km, but at very high resolution in the vertical. Unfortunately, the relative humidity measurement is based on temperature readings from a wet-bulb/dry-bulb thermistor pair; at the freezing point the crystallization of the water film covering the wet-bulb thermistor releases latent heat, warming the wet bulb and introducing a spurious spike into the apparent relative humidity record. Also there are differential phase lags between the responses of the wet-bulb, dry-bulb, and pressure sensors, leading to hysteresis errors: the computed relative humidity at a given altitude will depend on whether the balloon is ascending or descending. *Bruegge et al.* [1992] estimate that the integrated water column amounts derived from these sondes are certain to at best ±13%. For these reasons we elected to use the nonlocal sondes from Dodge City and Topeka in preference to the vertically truncated FIFE soundings.

4. Results

4.1. FIFE Validation

For each of the 11 navigable NOAA 11 images listed in Table 2, we located the eight pixels within each image which contained the IRT (infrared thermometer) ground sites. This was done by scanning the image's latitude/longitude grid to find that pixel which minimizes the great circle arc distance to the IRT (latitude, longitude) coordinate. We then applied the navigation correction, taking into account whether the image was for a descending or ascending pass, to translate from the nominal IRT position to the corrected IRT position. The raw channel 4 and 5 counts at this revised position were converted to calibrated at-satellite radiances, I_4 and I_5.

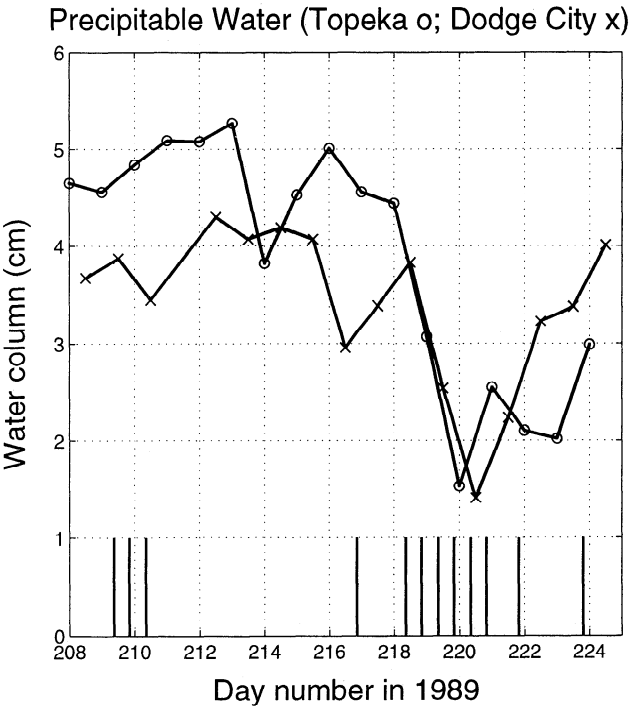

Figure 5. Time series of the precipitable water over Topeka (70 km east of FIFE) and Dodge City (340 km southwest of FIFE). These water column amounts were computed by integrating the specific humidity with respect to pressure using the Topeka and Dodge City radiosondes. The vertical bars on the time axis show the overpass times of the 12 AVHRR images listed in Table 2.

Using the Dodge City radiosonde whose launch date matched the date of the satellite pass, we ran the DWV-LST algorithm, iterating the water profile until the emissivity curves intersected at a common value of $\varepsilon_4 = \varepsilon_5 = 1.0$. This intersection point defined the retrieved surface temperature, T_x. This process was repeated for each of the eight IRT sites for each of the 11 images, for a total of 86 IRT/DWV-LST matchups (the two cloud-contaminated pixels listed in Table 2 were excluded). Assuming the IRT point measurement T_s can be meaningfully compared with the AVHRR-scale LST-DWV retrieval T_x, we computed the bias $(T_x - T_s)$ and the rms (standard deviation of this difference) errors for each matchup. The results are presented in Table 3 and Figure 6.

The day and night statistics are quite distinct. For the five night passes, the bias errors are small and posi-

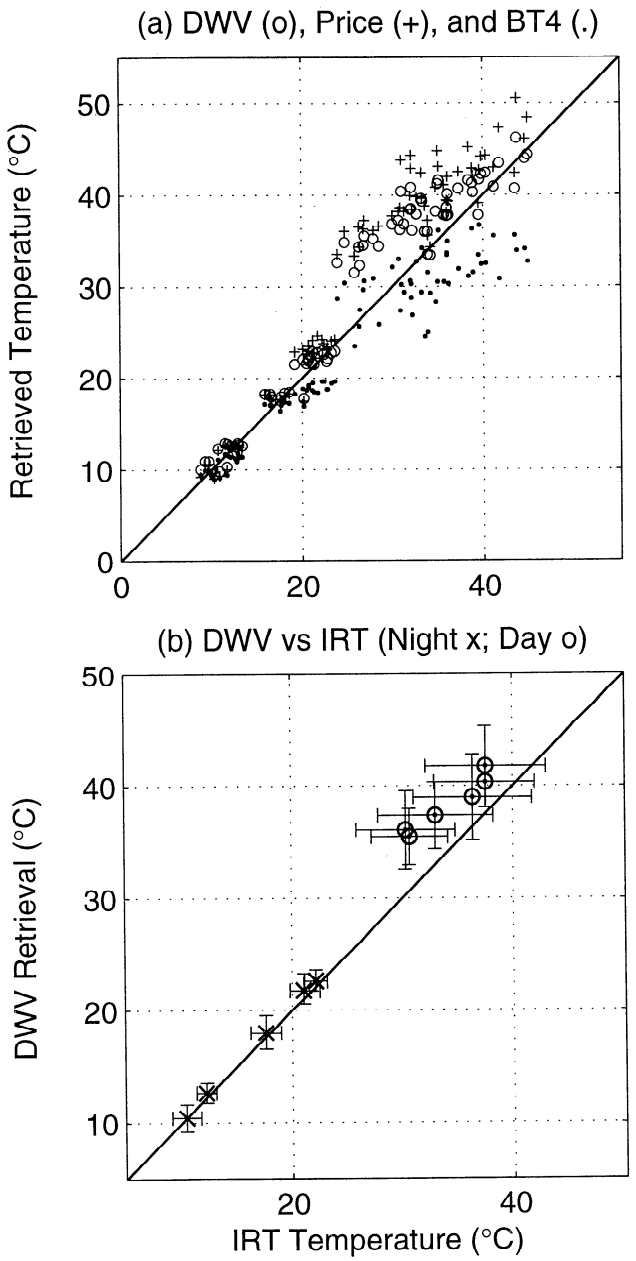

Figure 6. Comparison of retrieved surface temperatures with IRT ground measurements. (a) Circles are DWV-LST retrievals; plus signs are Price predictions (equation (9)); dots are channel 4 brightness temperatures. (b) DWV-LST retrievals averaged over the eight IRT sites for each of the 11 passes. Each vertical error bar shows the standard deviation in the eight DWV values for a given pass; the matching horizontal error bar is the standard deviation in the eight IRT measurements for that pass.

tive, with an average bias of +0.39 (T_x overestimates T_s by this amount) and average rms error of 1.11 K, while for the six day passes, the average bias and rms values are +4.09 and 3.10 K respectively. The fact that the daytime rms errors are about three times larger than for nighttime is not unexpected, given the very large spatial variability in daytime surface temperatures. However, the order-of-magnitude increase in bias from night to day requires some explanation. While the night bias is comfortably within the ±0.55 K AVHRR calibration uncertainty [*Weinreb et al.*, 1990], the day bias is well outside the calibration error band, and its error bar of ±3.10 K does not overlap zero bias.

Other authors [*Goetz et al.*, 1995; *Kalluri and Dubayah*, 1995] have also reported radiometric LST retrievals for FIFE which seem to be biased high relative to the IRT surface measurements. The most plausible explanation is that the IRT sites are not representative of the FIFE region, since the IRT sites are typically fenced off and therefore well vegetated compared with the surrounding prairie which is grazed and/or burned [*Kalluri and Dubayah*, 1995]. This means that the IRT field of view (area ~0.3 m^2) will be predominantly of vegetation, while the AVHRR view (area ~1 km^2) will contain a much larger proportion of sparsely vegetated land. During the day, the exposed ground (litter, soil) would be expected to be warmer than the plant canopy, so the satellite radiometer retrievals also will be warmer, and thus positively biased, relative to the IRT measurements.

If there is a vegetation-induced temperature bias, then we would expect the bias error to diminish with satellite scan angle, since at larger angles the satellite radiometer receives more radiation from the canopy and less from the ground [*Hall et al.*, 1992; *Vining and Blad*, 1992; *Prata*, 1994]. We plotted the DWV-LST bias errors as a function of scan angle for the six day and five night passes (not shown here), and found the best fit line through the day pass results seems to support the differentially vegetated hypothesis: bias errors are smaller at larger scan angles. At night the temperatures are more homogeneous, the errors are smaller, and any vegetation effects are probably negligible.

How well does DWV-LST perform compared with the other retrieval methods? The FIFE CD-ROMs used the *Price* [1984] algorithm. We assume its performance is representative of the equation (1) class of single-line, fixed-coefficient algorithms. Comparisons of DWV with the more recent atmospherically correcting methods of *Harris and Mason* [1992] and *Sobrino et al.* [1993, 1994] will be presented in a future paper.

For the case of unity emissivity, the Price formula simplifies to a linear combination of the at-satellite brightness temperatures in channels 4 and 5:

$$T_{\text{Price}} = T_4 + 3.33(T_4 - T_5) \tag{9}$$

Table 3. Average Bias and rms Errors for DWV, Price, and BT4 Methods

	Night (Five Passes)		Day (Six Passes)	
Method	Bias	rms	Bias	rms
DWV	+0.39	1.11	+4.08	3.10
Price	+0.73	1.14	+6.13	3.13
BT4	−1.52	1.13	−3.32	3.46

The data are in kelvins. BT4 is the AVHRR channel 4 brightness temperature. The number of matchups is 39 for night and 47 for day.

Since some authors have noted that T_4 sometimes gives quite good nighttime LST retrievals, we also computed the bias and rms errors for $(T_4 - T_s)$. The comparative results for DWV, Price, and T_4 are shown in Table 3. All three methods have very similar rms values, but very distinct bias values. On average, T_4 underestimates the IRT reading by 1.5 K at night, and by 3.3 K during the day, indicating that the atmospheric attenuation is not negligible. If the previously described vegetation effect is real (so that the IRT daytime readings need to be increased by ~4 K to match the DWV-LST values), then T_4 could be underestimating the surface temperature by as much as 7 K.

We found that the Price biases vary markedly from pass to pass. Figure 5 shows that the water vapor is strongly varying, and thus the assumed linearization of transmissivity with respect to water vapor content, which is the basis of the Price split-window algorithm, is not likely to be valid. A fixed-coefficient algorithm is therefore not expected to perform well, except in some time-averaged sense (if the coefficient is properly chosen, then over time the bias errors should average to zero, even though the bias error on any given day might be unacceptably large). The fact that Price performs better at night than during the day is probably due to the nighttime formation of a strong inversion in the vertical profiles for water vapor and temperature as reported by *Platt and Prata* [1993]. The radiance from this warm moist layer of air tends to compensate for the atmospheric attenuation in the cooler layers above. Under these conditions, T_4 can be a good predictor of T_s since the $(T_4 - T_5)$ correction term is small. The night passes of August 6, 7, and 8 (see Table 1) exhibit closely similar values for T_s, T_4, and T_5 for the eight land targets. Interestingly, the Tuttle Creek pixels show quite dissimilar T_4, T_5 values, suggesting that for water targets the nighttime vertical profiles for temperature and water vapor are quite different from those prevailing over land.

4.2. DWV Sensitivity Analysis

This section addresses the question: How sensitive is DWV to errors or uncertainties in surface emissivity and the first-guess atmospheric profile? The atmospheric contribution is examined first with respect to the choice of radiosonde profile, and second, with respect to synthetic perturbations in the profiles for water vapor, aerosol content, and atmospheric temperature.

4.2.1. Surface emissivity variations. The present work assumes $\varepsilon_4 = \varepsilon_5 = 1.00$. While this may be a reasonable assumption for moist (e.g., dew-covered) vegetation, it is not expected to be valid for dry, sparsely vegetated regions. In order to quantify the sensitivity of the retrieved surface temperature to variations in surface emissivity, we defined a sensitivity parameter $\Delta T/\Delta\varepsilon$, with units of kelvin change per percent change in emissivity. This was estimated, for a given atmosphere, by measuring the slope of the T_s versus ε curve (i.e., transpose of Figure 2) at the point $\varepsilon_4 = 1.00$. Typical values for a moist atmosphere (~4 cm water column) were $\Delta T/\Delta\varepsilon \sim -0.3$ K/%, i.e., if the assumed emissivity changes from 1.00 to 0.95, a 5% reduction, the retrieved surface temperature increases by $5 \times 0.3 = 1.5$ K. The sensitivity to ground conditions is stronger in drier atmospheres, e.g., for water column ~1.5 cm, $\Delta T/\Delta\varepsilon \sim -0.6$ K/%. We also investigated the sensitivity to spectral differences in emissivity (e.g., $\varepsilon_4 = 1.00$, $\varepsilon_5 = 0.95$), and found broadly similar results, although these latter findings must be regarded as preliminary and requiring further work.

4.2.2. Choice of radiosonde. How sensitive are the DWV-LST retrievals to choice of radiosonde? To answer this question we repeated the analysis for all 86 IRT/AVHRR pixel matchups using the Topeka sondes in place of those from Dodge City. Figure 5 shows that the Topeka and Dodge City water vapor burdens differ by as much as 20%; in addition, because there is a 12-hour disparity between launch times at the two sites, the temperature profiles are also likely to be quite different at the lower altitudes. By design, the DWV algorithm assumes that the temperature profiles are correct, and that any unphysical emissivity intersections are purely the result of inaccurately known water vapor profiles. Thus the algorithm attempts to compensate for temperature profile errors by adjusting the water profiles. The impact of imperfectly known temperature profiles is discussed later in this section.

Figure 7 plots the difference between the Topeka-DWV and the Dodge City-DWV LST predictions. Surprisingly, we see that the DWV retrievals are quite insensitive to choice of radiosonde, with the two sets of predictions typically lying within ±1 K of each other. There is a sign change between night and day, but the standard deviation of the differences is not substantially larger for the day passes: 0.45 K for night, 0.47 K for day. This result is markedly different from that ob-

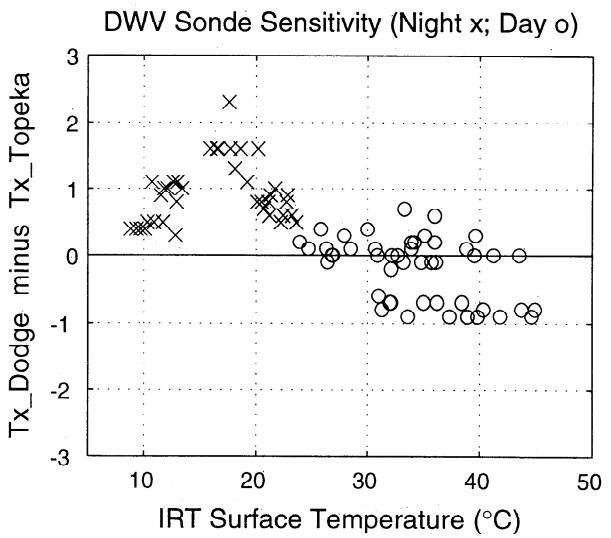

Figure 7. Sensitivity of DWV-LST retrieval to choice of radiosonde. Because of differences in location, launch time, temperature, and water vapor profiles of the Dodge City and Topeka sites (see Figure 5), the two sets of DWV-LST retrievals are not expected to be identical.

tained when the DWV retrievals were compared with the IRT ground values (Table 4, Figure 6); in the IRT comparison, the daytime rms differences were typically three times larger than the nighttime values.

Because dissimilar sondes from Dodge City and Topeka produce closely similar DWV-LST retrievals over FIFE, it is tempting to regard the ~0.47 K rms difference as an indicator of the absolute accuracy of the DWV method. However, much more validation work is required before we can be confident of this accuracy claim.

4.2.3. Aerosols, water vapor, atmospheric temperature. An investigation into the sensitivity of the DWV method to inaccuracies in the assumed vertical profiles for aerosols, water vapor, and atmospheric temperature was conducted by *Smith* [1993] using AVHRR data obtained over ocean and asssuming unity emissivity. Since for the present FIFE validation work we take $\varepsilon_4 = \varepsilon_5 = 1$, the Smith sensitivity conclusions should be broadly applicable here. Smith's study examined 30 AVHRR passes which were coincident with sea temperature data from a buoy moored off the west coast of Tasmania, Australia, for July–August 1987.

Smith obtained an estimate of the effect of aerosol uncertainties by running LOWTRAN-7 with its "no haze", "maritime", and "navy maritime" aerosol settings. Relative to the zero-aerosol (no haze) case, the maritime setting raised the retrieved DWV-SST by an average of 0.08 K, while the navy maritime setting raised the SST retrieval by about 0.3 K. (The effects of volcanic aerosols are expected to be more significant, but were not investigated.) Since both values are well within the ±0.55 K rms calibration accuracy of AVHRR, and because we have no information on aerosol profiles over FIFE, we ignore the influence of aerosols in the present work.

To quantify the impact of errors in the profiles for water vapor and atmospheric temperature, Smith computed a climatological reference atmosphere by averaging an archive of 5723 radiosonde profiles from the Tasmanian region. He then perturbed the reference by increasing (+) and decreasing (−) the water vapor (W) and temperature (T) values at each level by 0.25 of the range of the variable at that level to create four test atmospheres W_-T_0, W_+T_0, W_0T_-, W_0T_+. The DWV-SST retrievals using the test atmospheres were compared with those from the reference W_0T_0 atmosphere. The perturbed water vapor profiles W_-T_0, W_+T_0 produced SSTs which were only marginally different from the reference runs (bias errors < 0.05 K). While the results from the cooled atmosphere W_0T_- were similar (bias error of 0.02 K), those from the heated atmosphere W_0T_+ exhibited significant errors (−0.64 K bias, 0.93 K rms). Smith argued that a heated atmosphere raises the computed top-of-atmosphere radiance, exceeding the true radiance measured by the satellite. DWV attempts to compensate by loading water into the atmosphere to reduce the transmittance, thereby increasing the water vapor radiance and decreasing the surface contribution. The result is an artificially lowered SST retrieval. We conclude from Smith's study that DWV retrievals can be compromised if there are large errors in the assumed temperature profile.

Table 4. Split-Window Coefficients Derived from DWV-LST

	Night (Five Passes)		Day (Six Passes)	
Pass	Mean	s.d.	Mean	s.d.
1	2.51	0.14	2.52	0.09
2	2.42	0.13	2.81	0.04
3	4.64	1.89	2.65	0.03
4	4.40	0.90	2.75	0.23
5	5.42	0.92	2.46	0.18
6	...	...	2.60	0.24
Average	3.88	0.80	2.63	0.14

Here, s.d. denotes standard deviation.

5. Using DWV-LST to Derive Split-Window Coefficients

Unlike the one-line algorithm of (1), the DWV-LST method is computationally expensive. Typically, for each IRT/AVHRR pixel matchup, about seven DWV iterations were required: four iterations to bracket the $(\varepsilon_{\text{req}}, T_x)$ root, plus a further three iterations to polish the root to the desired level of precision; each iteration involved 12 LOWTRAN-7 runs (see section 2.3, step 4) for a total CPU time of about 30 s per pixel on a DEC Alpha 3000/800 computer. Extrapolating these run times to a 256- by 256-pixel image implies a time budget in excess of 500 hours.

Is it possible to craft a hybrid algorithm which preserves the accuracy and precision of the DWV method but which runs at split-window speeds? We plotted graphs of T_{Price} versus T_x for each of the 11 passes (not shown here) and observed that for each pass, there seemed to be a linear relationship between T_{Price} and T_x, but that the gradients for each of these varied from pass to pass. This suggested to us that it should be possible to use DWV to derive a split-window algorithm whose coefficient (a, in (1)) is tuned on a per-pass basis. Replace T_s in (1) with the DWV-LST value T_x, and solve for a; then compute its average value from a small but representative number of AVHRR pixels:

$$a(t) = \frac{1}{N}\sum_{j=1}^{N}(T_{s,j} - T_{5,j})/(T_{4,j} - T_{5,j}) \qquad (10)$$

For our demonstration we chose the $N = 8$ IRT pixels. The t argument in $a(t)$ emphasizes that the coefficient is (slowly) time-varying (on atmospheric timescales; we assume it is effectively constant within a given pass).

The results of this regression fit are shown in Table 4 and Figure 8.

Table 4 shows that the DWV-derived split-window coefficients for the night passes are highly variable, while those for the day passes are comparatively stable. It is interesting to note that the *Price* [1984] coefficient of 3.33 (equation(9)) is bracketed between the averaged day value of 2.63 and the averaged night value of 3.88, but that for none of the 11 passes does a coefficient of 3.33 seem appropriate. Figure 8 demonstrates the quality of the split-window fit to the DWV-LST value. The residual errors in Figure 8b show agreement within ±1 K, with an rms difference of 0.30 K. These encouraging results suggest that it is feasible to use DWV-LST to compute dynamically tuned split-window coefficients whose performance is only marginally less accurate than the full DWV. As pointed out by a reviewer, a three-coefficient regression fit should perform better than the single-coefficient method developed here for demonstration purposes.

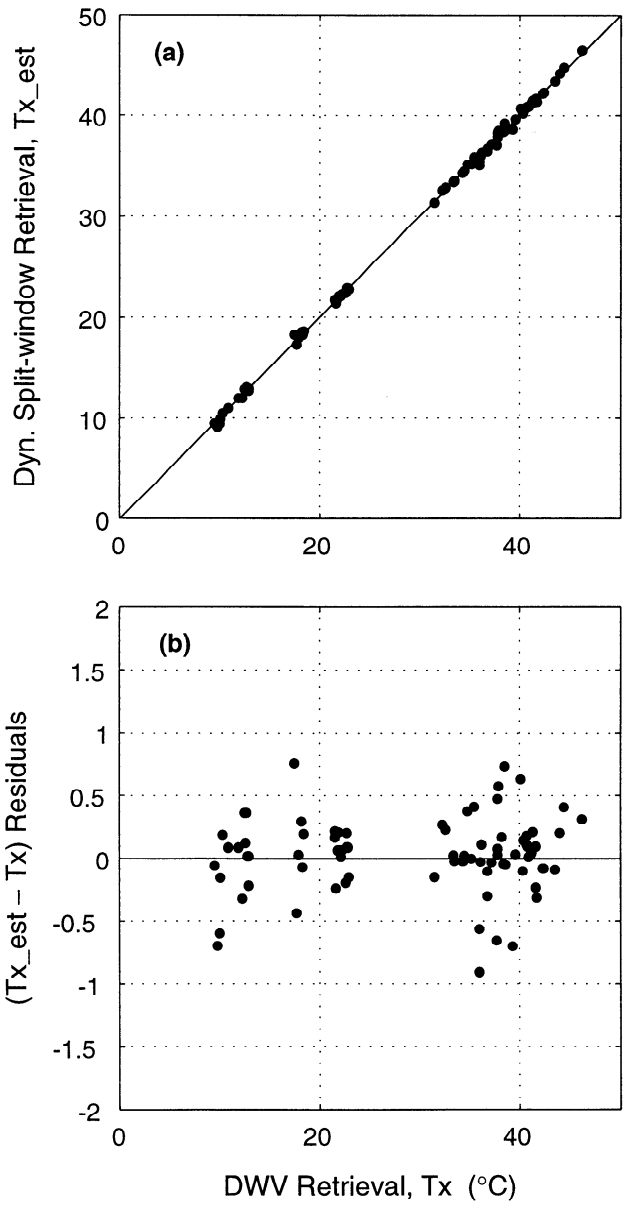

Figure 8. Feasibility of a dynamic split-window LST algorithm. For each pass, a new $(T_4 - T_5)$ coefficient is computed to allow T_x to be estimated from a linear combination of T_4 and T_5 (see Table 4). (a) Dynamic split-window predictions of T_x. (b) Residual error in dynamic split-window relative to DWV-LST.

6. Discussion and Conclusions

We have described a general, graphical scheme for determining upper and lower bounds for land surface temperatures retrieved from AVHRR radiance measurements. Because the retrieval problem is underconstrained, some knowledge of surface emissivity is required. In the absence of such knowledge, information about land classification will enable a reasonable guess for the emissivity range, e.g., $0.95 \leq \varepsilon \leq 0.99$ for vegetated surfaces. To correct for atmospheric effects, we have described a generalization of the dynamic water vapor (DWV) algorithm which was originally developed to retrieve sea surface temperatures in the presence of strongly varying water vapor.

To demonstrate our method, we applied the DWV philosophy to the 11 AVHRR images recorded during the fifth intensive field campaign of FIFE in July and August 1989. We compared our LST retrievals with the point surface measurements returned by a set of eight infrared thermometers (IRTs) which had been calibrated assuming a surface emissivity of unity. For the five night passes, the DWV-IRT comparisons showed average bias and rms errors of +0.39 and 1.11 K, respectively, while for the day passes the corresponding errors were +4.09 and 3.10 K. The rms errors are in reasonable accord with the spatial variability in IRT ground temperatures. The significant positive bias for the daytime DWV retrievals is consistent with the notion that the AVHRR view is not a scaled-up replication of the IRT view, even after the FIFE images have been corrected for navigation errors.

We compared the performance of DWV-LST with that of *Price* [1984], a traditional one-line split-window algorithm which uses a fixed coefficient. While the Price rms errors were quite similar to those for DWV, the bias performances were significantly worse: +0.74 K for night passes, and +6.13 K for day passes.

Because the DWV method uses a radiosonde to supply the first guess for the atmospheric state, we tested the algorithm for sensitivity to changes in radiosonde selection. DWV-LST predictions based on Dodge City sondes were compared with those based on sondes from Topeka. We found that the two sets of predictions agreed to within an rms difference of 0.47 K.

We presented a sensitivity analysis of DWV over ocean which supports the notion that as long as the temperature profile is known accurately, DWV is quite robust to the choice of first-guess water vapor profile. One means of obtaining this extra temperature information could be from an additional radiance measurement

made in the vicinity of channels 4 and 5. Assuming a blackbody surface this would give three equations and three unknowns (surface temperature, atmospheric water content, average atmospheric temperature). The launch of the moderate-resolution imaging spectrometer (MODIS) instrument in 1998 will provide several extra infrared channels in the 8–14 μm range, and one or more of these may enable the atmospheric temperature retrieval we require. This is the focus of ongoing research.

The DWV-LST method is computationally time expensive. To speed LST retrievals, we investigated the feasibility of establishing a dynamically tuned split-window coefficient which could be computed and applied on a per-pass basis. These feasibility tests showed that it is possible to replicate the DWV-LST retrievals to within an rms error of 0.30 K using a locally tuned split-window algorithm.

With the significant exception of the new algorithms of *Harris and Mason* [1992] and *Sobrino et al.* [1993, 1994], the usual theoretical derivation of the split-window algorithm assumes dry atmospheres and weak atmospheric absorption, allowing linearization of the transmissivity and the use of a globally applicable constant coefficient. However, since water column amounts over Topeka and Dodge City (and almost certainly over FIFE) sometimes exceeded 4 cm, the weak absorption approximation would not generally be valid. For high water vapor content, it is always necessary to expand the transmissivity to at least second order, thereby introducing a water vapor dependence into the a coefficient. Provided that the water column varies by not more than ~10% across the image, the adoption of a constant per-pass a coefficient seems to render LST retrievals of acceptable accuracy. We estimate this 10% figure from the magnitude of the typical water vapor variations computed by DWV, though a full water column sensitivity analysis is still to be done to establish quantitative bounds on expected split-window accuracies in the presence of large water vapor concentrations.

Acknowledgments. This research was supported in part by a grant from the New Zealand Lottery Science Research Committee. We thank Keith Oleson for several useful and enjoyable discussions regarding navigation of the AVHRR FIFE images. We also acknowledge the several very helpful suggestions made by anonymous reviewers.

References

Anding, D., and R. Kauth, Estimation of sea surface temperatures from space, *Remote Sens. Environ., 1*(4), 217–220, 1970.

Becker, F., and Z.-L. Li, Towards a local split window method over land surfaces, *Int. J. Remote Sens., 3,* 369–393, 1990.

Blad, B. L., E. A. Walter-Shea, C. J. Hays, and M. A. Mesarch, Calibration of field reference panel and radiometers used in FIFE 1989, *AgMet Progr. Rep. 90-3,* Dep. of Agric. Meteorol., Univ. of Neb., Lincoln, 1990.

Bruegge, C., J. E. Conel, R. O. Green, J. S. Margolis, R. G. Holm, and G. Toon, Water vapor column abundance retrievals during FIFE, *J. Geophys. Res., 97,* 18,759–18,766, 1992.

Cooper, D. I., and G. Asrar, Evaluating atmospheric correction models for retrieving surface temperatures from the AVHRR over a tallgrass prairie, *Remote Sens. Environ., 27,* 93–102, 1989.

Goetz, S. J., R. N. Halthore, F. G. Hall, and B. L. Markham, Surface temperature retrieval in temperate grassland with multiresolution sensors, *J. Geophys. Res., 100,* 25,397–25,410, 1995.

Hall, F. G., K. F. Huemmrich, S. J. Goetz, P. J. Sellers, and J. E. Nickeson, Satellite remote sensing of surface energy balance: Success, failures and unresolved issues in FIFE, *J. Geophys. Res., 97,* 19,061–19,090, 1992.

Harris, A. R., and I. M. Mason, An extension to the split-window technique giving improved atmospheric correction and total water vapour, *Int. J. Remote Sens., 13*(5), 881–892, 1992.

Kalluri, S. N. V., and R. O. Dubayah, Comparison of atmospheric correction models for thermal bands of the advanced very high resolution radiometer over FIFE, *J. Geophys. Res., 100,* 25,411–25,418, 1995.

Kneizys, F.X., et al., Users guide to LOWTRAN-7, *Tech. Rep. AFGL-TR-88-0177,* Opt./Infrared Technol. Div., U. S. Air Force Geophys. Lab., Hanscom Air Force Base, Mass., 1988.

Li, Z.-L., and F. Becker, Feasibility of land surface temperature and emissivity determination from AVHRR data, *Remote Sens. Environ., 43,* 67–85, 1993.

McMillin, L. M., Estimation of sea surface temperatures from two infrared window measurements with different absorption, *J. Geophys. Res., 80,* 5113–5117, 1975.

Ottle, C., and D. Vidal-Madjar, Estimation of land surface temperature with NOAA 9 data, *Remote Sens. Environ., 40,* 27–41, 1992.

Palluconi, F., A. B. Kahle, G. Hoover, and J. E. Conel, *The Spectral Emissivity of Prairie and Pasture Grasses at Konza Prairie, Kansas,* pp.77 78, Am. Meteorol. Soc., Boston, Mass., 1990.

Ph.D. Associates, Inc., *Digital Chart of the World in ASCII* [CD-ROM], Toronto, Ont., Canada, 1994.

Platt, C. M. R., and A. J. Prata, Nocturnal effects in the retrieval of land surface temperatures from satellite measurements, *Remote Sens. Environ., 45,* 127–136, 1993.

Prabhakara, C., G. Dalu, and V. G. Kunde, Estimation of sea surface temperature from remote sensing in the 11–13 μm window, *J. Geophys. Res., 79,* 5039–5044, 1974.

Prata, A. J., Land surface temperatures derived from the AVHRR and ATSR, 1, Theory, *J. Geophys. Res., 98,* 16,689–16,702, 1993.

Prata, A. J., Land surface temperatures derived from the AVHRR and ATSR, 2, Experimental results and validation of AVHRR algorithms, *J. Geophys. Res., 99,* 13,025–13,058, 1994.

Press, W. H., S. A. Teukolsky, W. T., Vetterling, and Flannery, B. P. *Numerical Recipes in C: The Art of Scientific Computing,* 2nd ed., Cambridge Univ. Press, New York, 1992.

Price, J. C., Land surface temperature measurements from the split window channels of the NOAA 7/AVHRR, *J. Geophys. Res., 89,* 7231–7237, 1984.

Salisbury, J. W., and D. M. D'Aria, Emissivity of terrestrial materials in the 8–14 μm atmospheric window, *Remote Sens. Environ., 42,* 83–106, 1992.

Sellers, P. J., F. G. Hall, G. Asrar, D. E. Strebel, and R. E. Murphy, An overview of the First International Satellite Land Surface Climatology Project (ISLSCP) Field Experiment (FIFE), *J. Geophys. Res., 97,* 18,345–18,371, 1992.

Smith, P. J., The dynamic water vapor algorithm for SST

retrievals, M.Sc. thesis, 170 pp., Univ. of Waikato, Hamilton, New Zealand, Feb. 1993.

Sobrino, J. A., and V. Caselles, A methodology for obtaining the crop temperature from NOAA 9 AVHRR data, *Int. J. Remote Sens., 12,* 2461–2475, 1991.

Sobrino, J. A., C. Coll, and V. Caselles, Atmospheric correction for land surface temperatures using NOAA 11 AVHRR channels 4 and 5, *Remote Sens. Environ., 38,* 19–34, 1991.

Sobrino, J. A., Z. L. Li, and M. P. Stoll, Impact of the atmospheric transmittance and total water vapor content in the algorithms for estimating sea surface temperatures, *IEEE Trans. Geosci. Remote Sens., 31*(8), 946–958, 1993.

Sobrino, J. A., Z. L. Li, M. P. Stoll, and F. Becker, Improvements in the split-window technique for land surface temperature determination, *IEEE Trans. Geosci. Remote Sens., 32*(2), 243–253, 1994.

Stewart, J. B., A study of areal average evapotranspiration by measuring and modeling its surface controls, in file /fife_1/document/sur_flux/sflux_eb.doc, FIFE vol. 1, *Surface Observations and Non-image Data Sets* [CD-ROM], NASA, Washington, D. C., 1994.

Steyn-Ross, D. A., M. L. Steyn-Ross, and S. Clift, Radiance calibrations for advanced very high resolution radiometer infrared channels, *J. Geophys. Res., 97,* 5551–5568, 1992.

Steyn-Ross, M. L., D. A. Steyn-Ross, P. J. Smith, J. D. Shepherd, J. Reid, and P. Tildesley, Water vapor correction method for advanced very high resolution radiometer data, *J. Geophys. Res., 98,* 22,817–22,826, 1993.

Strebel, D. E., D. R. Landis, K. F. Huemmrich, and B. W. Meeson, *Collected Data of the First ISLSCP Field Experiment,* vol. 1, *Surface Observations and Non-image Data Sets* [CD-ROM], NASA, Washington, D. C., 1994.

Strebel, D. E., D. R. Landis, J. N. Newcomer, D. van Elburg-Obler, B. W. Meeson, and P. A. Agbu, *Collected Data of the First ISLSCP Field Experiment,* vol. 2, *Satellite Imagery, 1978-1989* [CD-ROM], NASA, Washington, D. C., 1992.

Sugita, M. and W. Brutsaert, Wind velocity measurements in the neutral boundary layer above hilly prairie, *J. Geophys. Res., 95,* 7617–7624, 1990.

Vidal, A., Atmospheric and emissivity correction of land surface temperature measurements from satellite using ground measurements or satellite data, *Int. J. Remote Sens., 12,* 2449–2460, 1991.

Vining, R. C., and B. L. Blad, Estimation of sensible heat flux from remotely sensed canopy temperatures, *J. Geophys. Res., 97,* 18,951–18,954, 1992.

Weinreb, M. P., G. Hamilton, S. Brown, and R. J. Koczor, Nonlinearity corrections in calibration of advanced very high resolution radiometer infrared channels, *J. Geophys. Res., 95,* 7381–7388, 1990.

W. J. Emery, Department of Aerospace Engineering Sciences, University of Colorado, Boulder, CO 80302.

D. A. Steyn-Ross and M. L. Steyn-Ross, Department of Physics and Electronic Engineering, Room E3-20, University of Waikato, Gate 8, Hillcrest Road, Private Bag 3105, New Zealand. (e-mail: asr@waikato.ac.nz)

(Received April 10, 1996; revised December 18, 1996; accepted March 7, 1997.)